Research and Innovation Article
Salud UIS ISSN: 2145-8464

Tetramethylammonium Chloride and Dimethyl Sulfoxide improve SARS-CoV-2 detection in individual/pooled saliva samples with RT-qPCR

Cloruro de Tetrametilamonio y Dimetilsulfóxido mejoran la detección de SARS-CoV-2 en muestras de saliva individuales/agrupadas con RT-qPCR

Lina María Vera-Cala[1*], Nathaniel A. Navarro-Baron[1], Yordy S. Cangrejo-Useda[1], Luis A. Pardo-Diaz[1], Cristian E. Cadena-Caballero[1], Carlos J. Barrios Hernández[1,2], Francisco Martinez-Perez[1]

* limavera@uis.edu.co

1 Universidad Industrial de Santander, Bucaramanga, Santander, Colombia.
2 Instituto Nacional de Investigación en Informática y Automática, Grenoble, Francia

Recibido: 21/08/2025. Aprobado: 16/10/2025

Abstract

Introduction: RT-qPCR performance to detect SARS-CoV-2 varies because SNPs at primer/probe sites and RNA secondary structures (notably 5′/3′ UTR stem-loops) can hinder hybridization/polymerase elongation, altering Ct and fluorescence. A denaturant solution (DS: composed of Tetramethylammonium Chloride and Dimethyl Sulfoxide) can disrupt these structures and improves its detection. **Objective:** Evaluate the DS efficiency in RT-qPCR to SARS-CoV-2 detection from single and multiplex saliva samples in COVID-19 positive patients. **Methodology:** To establish the hybridization pattern, *in silico* analysis was carried out among primers and probes authorized by CDC (Centers for Disease Control and Prevention) with respect to the consensus region of SARS-CoV-2 *N* gen, and their secondary and tertiary structures were generated to establish variable regions. Individual and pooled RT-qPCR with DS reactions, were validated from total RNA from 20 of 40 saliva samples positive to SARS-CoV-2. **Results:** N1 consensus region of SARS-CoV-2 variants: Alfa, Beta, Delta, Gamma, GH490R, Lambda, Mu y Ómicron from 2021, exhibited a high variation respect to N2 region, but were located in bubbles near to a stem and in the spacer region. Individual RT-qPCR to N1 and N2 regions showed no significant statistical differences in Cts, however, they were lower, with a remarkable difference in fluorescence signal, to N1 region in pooled RT-qPCR reactions. **Conclusion:** The procedure evidences the advantages in the inclusion of DS in RT-qPCR to SARS-CoV-2 detection in saliva samples.

Keywords: SARS-CoV-2; Saliva Samples; RT-qPCR Multiplex; Coadjuvant Solution; RNA Secondary Structure.

Suggested citation: Vera-Cala LM, Navarro-Baron NA, Cangrejo-Useda YS, Pardo-Diaz LA, Cadena-Caballero CE, Barrios CJ, Martinez-Perez F. Tetramethylammonium Chloride and Dimethyl Sulfoxide improve SARS-CoV-2 detection in individual/pooled saliva samples with RT-qPCR. Salud UIS. 2025; 57: e25v57a33. doi: https://doi.org/10.18273/saluduis.57.e:25v58a33

Resumen

Introducción: El desempeño de la RT-qPCR para detectar SARS-CoV-2 varía porque los SNP en los sitios de cebadores/sondas y las estructuras secundarias del ARN (en particular, los bucles de tallo en las UTR 5′/3′) pueden obstaculizar la hibridación y la elongación de la polimerasa, alterando el Ct y la fluorescencia. Una solución desnaturalizante (DS; compuesta por cloruro de tetrametilamonio y dimetilsulfóxido) puede alterar estas estructuras y mejorar la detección. **Objetivo:** Evaluar el efecto de la SD en la eficiencia de la RT-qPCR para la detección de SARS-CoV-2 en muestras de saliva individuales o agrupadas de pacientes diagnosticados con COVID-19. **Metodología:** Se determinó *in silico* el patrón de hibridación entre los cebadores y sondas autorizados por el *CDC* (*Centers for Disease Control and Prevention*) respecto a la región consenso del gen *N* de SARS-CoV-2, además de generar su estructura secundaria para definir las posiciones variables. La validación de las RT-qPCR individuales y agrupadas con la SD se realizó con ARN total en 20 de 40 muestras de saliva positivas a SARS-CoV-2. **Resultados:** La región consenso del gen *N1* de las variantes de SARS-CoV-2: Alfa, Beta, Delta, Gamma, GH490R, Lambda, Mu y Ómicron del año 2021, presentó más variaciones respecto a la región *N2*, no obstante, se localizaron dentro de las burbujas adyacentes a un tallo y en la región espaciadora. Las RT-qPCR individuales para las regiones N1 y N2 con SD no mostraron Cts estadísticamente significativos, sin embargo, estos disminuyeron, con una diferencia notable en la señal de fluorescencia, para la región N1 en las reacciones de RT-qPCR agrupadas. **Conclusión:** El procedimiento confirma la ventaja de la inclusión de la SD en la RT-qPCR para detectar SARS-CoV-2 en muestras de saliva.

Palabras clave: SARS-CoV-2; Muestras de Saliva; RT-qPCR múltiples; Solución Coadyuvante; Estructura Secundaria del ARN.

Introduction

The SARS-CoV-2 virus, the causal agent of the coronavirus disease COVID-19, was first identified at the end of 2019 in Wuhan, China [1]. Given its transmission via the respiratory tract, the global infection rate became increasingly high, leading the World Health Organization [WHO] to declare a pandemic in 2020 [2]. To curb its spread, the WHO recommended diagnosing this disease using purified RNA from nasopharyngeal swabs through a One-Step Reverse Transcription Quantitative Real-time PCR [RT-qPCR]. For this purpose, diverse primers and probes for RT-qPCR were designed supported on the initial characterization of the SARS-CoV-2 genome, which is a positive-sense single-stranded RNA of approximately 30 kb, containing 10 genes [1,3]. The Charité-Berlin protocol, which is widely recommended by the WHO, targets regions of the genes coding for RNA-dependent RNA polymerase [*RdRp*], Envelope protein [*E*] and Nucleocapsid phosphoprotein (*N*) [4]. Another diagnostic kit, designed by the Centers for Disease Control and Prevention-USA [CDC], utilizes two regions of the *N* gene and has proven successful in occupational medicine for singleplex and/or multiplex RT-qPCR to single and/or pooled nasopharyngeal swab samples [5,6]. Meanwhile other diagnostic kits use regions of the Spike (*S*) gene [7].

Despite the widespread application and accuracy of RT-qPCR for SARS-CoV-2 detection, previous studies on other RT-PCR methods have reported that the procedure may yield false negative results or low-quality amplification signals, leading to incorrect viral sample detection [8]. This is due to alterations in the hybridization pattern between the primers or probes caused by single nucleotide polymorphism in the target regions of the viral variants [9,10] and/or the polymerization capacity of DNA polymerase affected by the formation of RNA or DNA secondary structures that regulate gene expression [11].

A notable feature of the SARS-CoV-2 genome is the folding at the 5' and 3' genome untranslated regions, creating secondary stem-loops structures involved in regulating the translation of the first gene and the genome's half-life, respectively [12]. Additionally, certain viral RNA stems induce Programmed Ribosomal Frameshift in the *ORF1a* and *ORF1b* genes, altering translation at the stop codon to generate *ORF1ab*, a component of the viral RNA polymerase [13].

To address the challenges associated with RNA structures, we implemented a Denaturing Solution (DS) to prevent RNA folding in RT-qPCR, which contains Tetramethylammonium Chloride (TMAC) and Dimethyl Sulfoxide (DMSO) due to their affinity to A-T and G-C canonical bonds, respectively [14]. In turn, the concentration of this DS was adjusted in accordance with the nucleotide composition of the SARS-CoV-2 genome, which is rich in A-T[1]. As a result, the DS facilitates the elimination of viral RNA secondary structures that could interfere with proper polymerization [15].

This innovative formulation was then incorporated into RT-qPCR protocol for the examination of nasopharyngeal swab samples, yielding an improved polymerization signal or multiplex for SARS-CoV-2 detection [15]. However, many patients found nasopharyngeal swab sampling inconvenient, and it is also resource-consuming given the skilled staff required for the procedure [16,17]. Then, implementing this approach for a large number of patients proved complex and costly [18,19]. In response to these limitations, procedures involving individual or pooled saliva samples were introduced [20], the effect of the DS on these procedures in individual or pooled RT-qPCR in saliva pools had not been assessed, therefore, the objective of this study was to demonstrate that including the DS in RT-qPCR for SARS-CoV-2 detection, using N1 and N2 primers and probes for their respective regions in the *N* gene, enhances the polymerization signal in saliva samples collected over a 6-month period in Bucaramanga, Colombia. Taken together, our findings are expected to contribute to a better interpretation of viral detection.

Methodology

Ethics Statement

This study was approved by the Comité de Ética en Investigación Científica de la Universidad Industrial de Santander. Furthermore, this research adhered to all bioethical standards of the Declaration of Helsinki, revised in 2013 [21].

Homology pattern to primers/probes N1-N2 regions of *N* gene

Consensus genomic sequences for SARS-CoV-2 variants Alpha, Beta, Delta, Gamma, GH490R, Lambda, Mu, and Omicron from the year 2021 were obtained from the public database of SARS-CoV-2 from Cadena Caballero et al., 2023 [22], with nucleotide frequency thresholds of 20% and 100%. Alignments with respect to the SARS-CoV-2 reference sequence [23] were conducted using the MEGA software version 11 with default parameter [24]. Afterward, the percentage of identity for N1 and N2 primers and probes from the CDC SARS-CoV-2 protocol [6] [2019-nCoV TaqMan RT-PCR Kit - Norgen Biotek Corp.], was calculated for the N1 and N2 regions from the *N* gene reference and SARS-CoV-2 variant genes in terms of nucleotide changes per position, as indicated by the Nomenclature Committee of the International Union of Biochemistry (NC-IUB):

$$\%ident = \frac{nucleotidechangesperposition \times 100}{\delta nucleotidesofprimers \wedge probes}$$

The total nucleotide combinations by position in the NC-IUB for N1 and N2 primers and probes of the *N* gene in SARS-CoV-2 variants were determined by constructing a matrix in a spreadsheet.

$$= IF[O[B3 = "B"; B3 = "D"; B3 = "H"; B3 = "V"]; 3; 0] + IF[O[B3 = "K"; B3 = "M"; B3 = "R"; B3 = "S"; B3 = "W"; B3 = "Y"]; 2; 0] + IF[B3 = "N"; 4; 0]$$

Where the number of nucleotide combinations was indicated by: K, M, R, S, W or Y = 2; B, D, H or V = 3; and N = 4.

RNA structures from N1-N2 regions of the *N* gene

The patterns of stem and stem-loop RNA secondary structures of N1, N2, and RNase P regions of the respective genes from the CDC detection kit [6] were generated in Mfold software version 2.3 with default parameters [25]. VARNA version 3.93 was used to visualize the RNA secondary structures and RNAcomposer version 1.0 was used to obtain the RNA tertiary structures [26,27].

RNA extraction from saliva samples

Saliva samples, including 40 positive and 10 negative samples of SARS-CoV-2, were donated by *Laboratorio Central de Investigaciones de la Facultad de Salud de la Universidad Industrial de Santander*, collected by this institution from January to June 2022. For each sample, cell lysis, and purification of total RNA was carried out from 200 μL, using mechanical disruption and separation with magnetic beads with the MagMAX™ Viral/Pathogen II kit [MVP II - 2000 RXN - Applied Biosystems – USA] using the software BindIt version 4 on the equipment the KingFisher Duo Prime [Catalog number: 5400110 - DNA/RNA extraction system] according to the manufacturer's instructions (Thermo Fisher Scientific – USA).

Denaturing Solution (DS) in individual and pooled RT-qPCR

The effect of DS in singleplex RT-qPCR for SARS-CoV-2 single saliva samples was assessed using the 2019-nCoV TaqMan RT-PCR Kit protocol (Ref. TM67100, Norgen Biotek – Canada) [6]. Total RNA extractions from 20 of the 40 positive samples were randomly selected, and two sets of reactions were conducted. The first set included DS, and each reaction was conducted in a 15 μl volume composed by: 2 μL of total RNA; 7.5 μL of 2x One-Step RT-PCR Master Mix; 1 μL of DS (636 mM TMAC – ABCAM USA) and 423 mM DMSO (Scharlab – Spain] dissolved in nuclease-free water to a final reaction concentration of 21.2 mM and 14.1 mM, respectively) [22]; 1.2 μL 2019-nCoV Primer & Probe Mix to N1, N2 or RNase P (per sample); and 3.3 μL nuclease-free water. The second reaction set did not include DS because it was controlled, therefore 4.3 μL nuclease-free water was used.

The One-Step RT-qPCR cycling conditions consisted of: first, a step at 50 °C for 30 minutes; second, a step at 95 °C for 3 minutes; third, 45 cycles distributed in two steps, one at 95 °C for 3 seconds and the other at 55 °C for 30 seconds. For this, a QuantStudio 1 real-time PCR system (No. A40427) was used in a 96-well block of 0.2 μL (Thermo Fisher Scientific, USA).

For multiplex RT-qPCR to pooled samples, total RNA was obtained following the previous procedure from 11 pools, each comprising 200 μL from 10 saliva samples randomly selected from the initial 50 samples. To generate each pool, 20 μL by negative (n-) and positive (n+) SARS-CoV-2 samples were mixed in a proportion of: 10 negative samples and 0 positive; 9 negative and one positive; and so on until 10 positive samples and 0 negative. The RT-qPCR set for each pool included the standard procedure: 2 μl of RNA sample mix from each pool, 7.5 μL of 2x One-Step RT-PCR Master Mix; 1 μL of DS as previous indicated; 1.2 μL from 2019-nCoV Primer & Probe Mix to N1 and the same volume to N2 Primer & Probe Mix; and 3.3 μL nuclease-free water. The second RT-qPCR set served as the control, so did not include DS and 4.3 μL of nuclease-free water was used instead. The same procedure was applied to RNase P, serving as the RT-qPCR control. The RT-qPCR Program was conducted as described above.

Statistical analysis

Box plot diagrams were generated using the Cycle threshold (Ct) distribution from each individual and pooled RT-qPCR set with and without DS, indicated as standard. Furthermore, a t-test was conducted to establish the statistically significant difference between the Ct average of the individual RT-qPCR with and without DS. Shapiro-Wilk and Levene's tests were also performed to evaluate the normality of the data and the homogeneity of the variances, respectively. In cases where the results did not exhibit a normal distribution, Wilcoxon-Mann-Whitney test (U-Test) was employed for group comparison between the Ct values groups. All statistical analyses were conducted in RStudio version 2023.03.0+386 and R version 4.2.2 [28,29].

Results

Homology pattern of N1-N2 primers/probes

At the 20% frequency threshold, consensus sequences for N1 in the variants Alpha, Beta, Delta1, Delta2, Gamma, and Mu, exhibited 100% identity with the corresponding primers and probes sequences recommended

by the CDC for SARS-CoV-2 detection via RT-qPCR. However, for GH490R, Lambda, and Omicron, the identity exceeded 97%. In contrast, the primer and probe sequences for the N2 region showed consistent identity across all SARS-CoV-2 variants. The consensus sequences with a 100% frequency threshold for primers and probes to the N1 region of Gamma, GH490R, Lambda and Omicron variants exhibited an average identity of 96%, Beta and Mu variants 72.1% on average, while Delta 1 and 2 showed the least identity (Table 1). The N1 primers and probes regions of the GH490R variant with a 20% frequency threshold, showed a nucleotide pair combination, whereas the Lambda and Omicron variants displayed a single change, according to NC-IUB nucleotide nomenclature. For other N1 regions in SARS-CoV-2 variants, including the N2 region, nucleotide changes were not determined (Table 1).

Table 1. Identity percentages and number of potential nucleotide changes for the SARS-CoV-2 variants from 2021 in N1 and N2 regions of *N* gene.

SARS-CoV-2 variant consensus	N1				N2			
	Threshold frequency 20%		Threshold frequency 100%		Threshold frequency 20%		Threshold frequency 100%	
	ID %	N1 Changes	ID %	N1 Changes	ID %	N2 Changes	ID %	N2 Changes
Alpha	100	0	60.3	32	100	0	75.4	17
Beta	100	0	70.6	22	100	0	88.5	8
Delta1	100	0	45.6	48	100	0	60.7	29
Delta2	100	0	32.4	68	100	0	52.5	40
Gamma	100	0	98.5	1	100	0	100	0
GH490R	97.1	2	97.1	2	100	0	100	0
Lambda	98.5	1	92.6	5	100	0	98.4	1
Mu	100	0	73.5	20	100	0	78.7	13

Note: Threshold frequency 20-100%: indicates the threshold employed to obtain consensus sequences for the SARS-CoV-2 variants sequences. ID %: indicates the percentage of identity for primers and probes designed to detect N1 and N2 region of *N* gene, for consensus sequences of SARS-CoV-2 variants. N1-N2 Changes: indicates the number of possible nucleotide combinations per position for the N1 and N2 region of *N* gene, of the SARS-CoV-2 variants consensus sequences.

For SARS-CoV-2 variants with a 100% frequency threshold in primers and probes for the N1 region, Delta 1 and 2 variants showed the most significant changes per position. Alpha and Beta variants showed 50.5 changes in average, and except for the Mu variant, the other nucleotide combinations in the consensus regions of the SARS-CoV-2 variants exhibited fewer than 10 changes per position (Suppl. Material 1). In the N2 region, the nucleotide combinations for all variants were similar to the N1 region, but the total number of combinations was lower. The Delta 1 and 2 variants had more than 100 nucleotide combinations, different for Gamma, GH490R, and Omicron variants, where the identity was the same as the reference sequence; while Alpha, Beta, and Mu showed an average of 24.3 nucleotide combinations (Suppl. Material 1).

Secondary and tertiary RNA structures for N1-N2 of the N gene

The secondary structures from the N1 region to all SARS-CoV-2 variants with a 20% frequency threshold generated the same structure, consisting of two stem-loop structures separated by 14 nucleotides. Notably, nucleotide combinations determined for GH490R were localized in the first loop of the first stem-loop and the region separating both stem-loops. Meanwhile Lambda and Omicron variants exhibited a T-C variation in the

same nucleotide position of the second loop from the first stem-loop. A similar RNA secondary structure was observed in the N2 region and the RNase P sequence amplicon, but the stem-loop pairs were continuous in both cases (**Figure 1**).

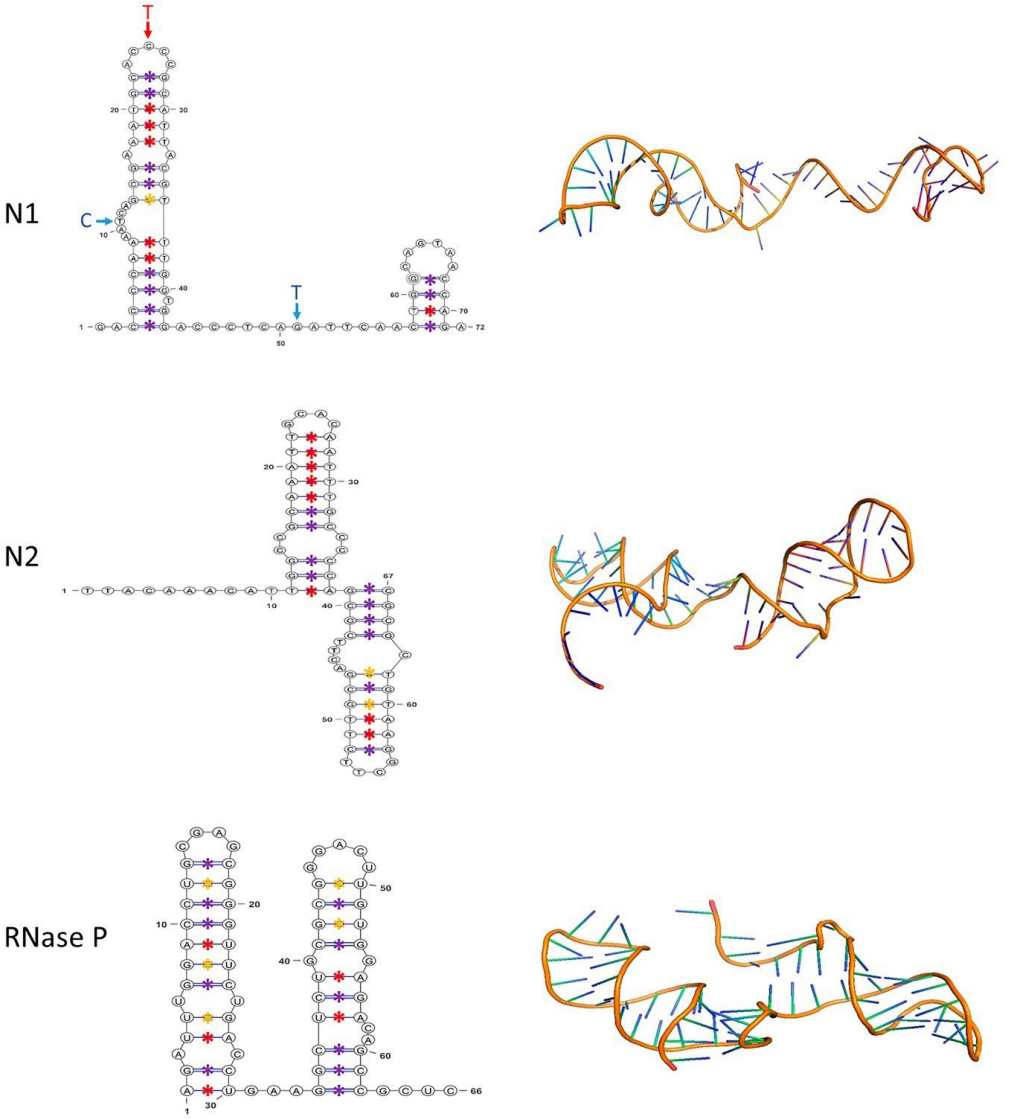

Fig. 1. Secondary and tertiary structures of the N1 and N2 regions of the SARS-CoV-2 *N* gene (NC_045512, Region: 28274-29533, position 14-86 and 891-957, respectively) and human *RNase P*. In the secondary structures of each of the amplicons (left), the nucleotide changes of the variant GH490R are indicated by blue letters and arrows, whereas the red arrow corresponds to Lambda and Omicron. Canonical A-T and G-C base pairings are shown with red and purple asterisks, respectively. Non-canonical Guanine-Thymine (G-T) pairings are marked with yellow asterisks. The tertiary structures of each region are displayed on the right

It is also worth noting that in the secondary structure of N1 and N2 regions of SARS-CoV-2 variants, the number of G-C base pairs in all stem-loop structures was determined at the beginning of each stem-loop. In contrast, A-T and non-canonical base pairs were preferably localized in the superior region of the stem-loop. In the RNase P stem-loops, the base pairs did not follow a specific pattern distribution (**Figure 1**).

DS improves SARS-CoV-2 detection by individual RT-qPCR

In the individual RT-qPCR for the N1 region, the expected result was obtained in 18 out of 20 samples, even after the addition of the DS. Moreover, amplifications for the N2 region and RNase P were successful in all samples with both treatments (Figure 2A). The average Ct values obtained for individual RT-qPCRs with DS and the standard solution showed differences for the N1 and N2 regions of the SARS-CoV-2 *N* gene and RNase P. With the inclusion of DS in single RT-qPCR for the N1 region and RNase P, the Ct average values were lower compared to the standard reaction. However, a slight increase in Ct average value was determined in presence of DS when targeting the N2 region via RT-qPCR (Figure 2A).

The Shapiro-Wilk's normality test revealed that the Ct values for individual RT-qPCR N1-DS (Ct mean= 21.48, SD= 8.44), N1-Standard (Ct mean= 22.32, SD=9.18), and RNase P-Standard (Ct mean= 22.65, SD= 2.07), did not follow a normal distribution. While the RT-qPCR of N2-DS (Ct mean= 23.82, SD= 5.19), N2-Standard (Ct mean= 23.21, SD= 4.73), and RNase P-DS (Ct mean= 21.88, SD= 1.72) Ct values exhibited a normal distribution. Furthermore, all RT-qPCR treatments had homogenous variances according to Levene's Test. However, according to our t-test analyses, there were no statistically significant differences between the Ct averages of the N2-DS and N2-Standard RT-qPCR. For groups without a normal distribution, U-Test results also showed no differences between the Ct average values (**Table 2**).

Table 2. The t-test and U-test results indicate no statistically significant differences between the Ct averages, *p-value= 0.05*.

Individual RT-qPCR	Shapiro-Wilk's normality test	Levene's Test	T-Test	Wilcoxon-Mann-Whitney test (U-Test)
N1-DS	0.001484*	0.7618	N.D	0.735
N1-Standard	0.01227*			
N2-DS	0.3507	0.5421	0.698	N.D
N2-Standard	0.604			
RNase P-DS	0.6378	0.8897	N.D	0.2012
RNase P-Standard	0.0415*			

Note: DS indicates RT-qPCR reactions with the Denaturant Solution. Standard indicates RT-qPCR reactions without the Denaturant Solution. Values with *, indicates Ct average without a normal distribution. N.D indicates non-determined test according to non-compliance their assumptions.

DS improve SARS-CoV-2 detection by pooled RT-qPCR

The pooled RT-qPCR for the N1/N2 regions in each of the 11 pooled samples and RNase P produced the expected result. The Ct average for N1/N2 regions and RNase P showed a decrease with the DS solution compared to the standard solution (**Figure 2B**). Notably, the onset of the Log phase in the RT-qPCRs was directly proportional to the number of positive samples within each pooled sample, and the number of cycles required to obtain their Ct was lower when DS was included in each pooled RT-qPCR. Moreover, the inclusion of DS showed a remarkable difference in the fluorescence signal, being higher than the signal obtained in the standard RT-qPCR (**Figure 3**).

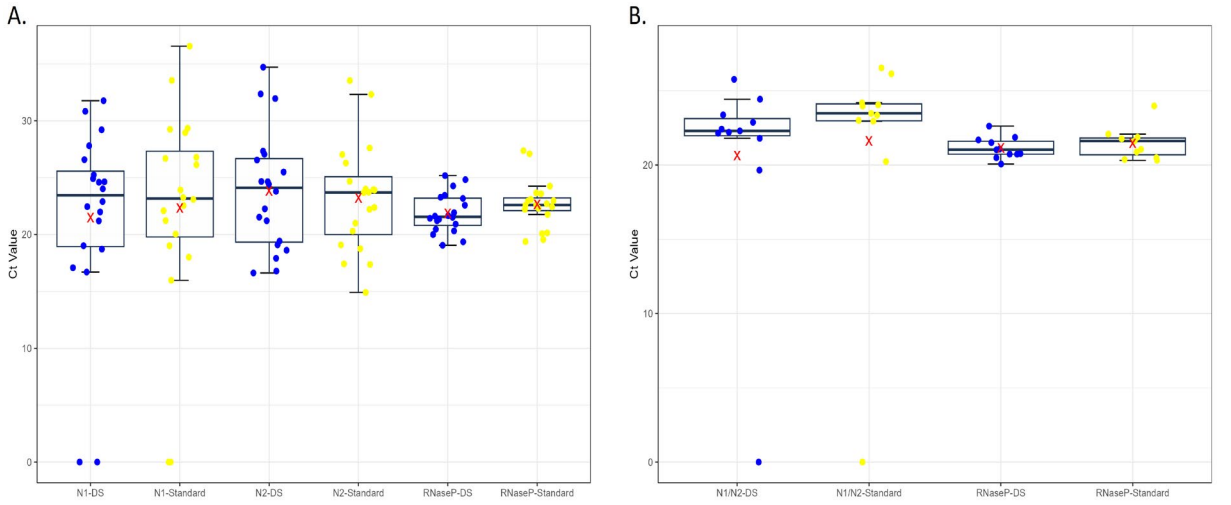

Fig. 2. Boxplot of Ct values from single (A) and pooled (B) RT-qPCR of the N1 and N2 regions of the SARS-CoV-2 *N* gene and human RNase P reaction set. The Ct average for each RT-qPCR set is marked with a red X. CT's value from sets with DS in the RT-qPCR are represented by blue dots, while the control set is indicated by yellow dots.

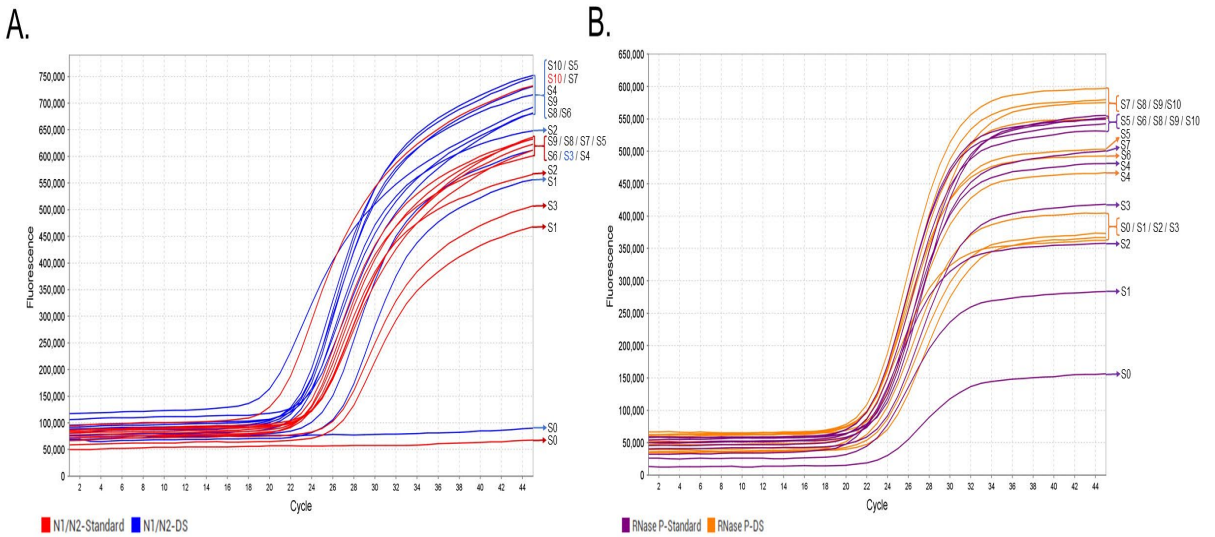

Fig. 3. Multiplex RT-qPCR for the characterization of the *N* gene and RNase P from SARS-CoV-2 using pooled saliva samples. The fluorescence signals emitted by the N1/N2 primers and probes targeting the respective SARS-CoV-2 *N* gene with DS are represented by blue curves, whereas the control RT-qPCR is indicated by red curves (A); and RNase P with DS are represented by orange curves, whereas the control RT-qPCR is indicated by purple curves (B). The numbers on the right side of the curve in both graphs indicate the number of positive SARS-CoV-2 RNA samples relative to the negative samples in the corresponding pool.

Discussion

Although RT-qPCR is widely regarded as the gold standard for SARS-CoV-2 diagnosis, it may occasionally yield false-negative results due to mutational patterns in new variants [30] and the secondary structures of viral RNA [12]. In this sense, the determination of those structures continues to be a challenge to establish its therapeutic potential and their elimination from RNA/DNA polymerase processes[31]; as demonstrated in the Hepatitis Delta Virus[32]

or the bacterium *Klebsiella pneumoniae*[33]. The findings from this study indicate that implementing DS to prevent RNA folding in RT-qPCR from saliva samples enhances the fluorescent signal and Ct values, both in single samples and multiplex pooled samples, for the N1 and N2 regions of the *N* gene used in the CDC protocol [6].

In silico analysis conducted in this study on some medically relevant SARS-CoV-2 variants during the COVID-19 pandemic previously reported [15], underscores the importance of comparing the identity between primers and probes respect to consensus regions employed in RT-qPCR for virus detection. In addition, the threshold frequency allows to determine the nucleotide polymorphism in a specific region of a gene or genome, which can be visualized in a consensus sequence based on the threshold frequency value [34]. In this study, the consensus regions obtained with a 20% threshold demonstrated a correct identity pattern for the N1 region in Alpha, Beta, Delta, Gamma, and Mu SARS-CoV-2 variants, while the N2 region showed complete identity across all eight variants. However, the N1 region of the GH490R, Lambda, and Omicron variants exhibited some changes in primers and probes. This nucleotide change pattern was corroborated with a couple of stem-loops formed in secondary structure that was the same to all variants. Notably, mutations in the N1 region of these three variants were located in the first stem-loop or spacer region, potentially leading to false-negative results due to their proximity to the hybridization region of primers and probes used in RT-qPCR, but without affecting their structure.

Moreover, *in silico* results with a 100% frequency threshold indicated that only the N2 region from Gamma, GH490R, and Omicron variants could be correctly identified, whereas the other variants and the N1 region from all variants had a high probability of generating false-negative results [35], particularly the Delta variant as reported previously [36].

The above was supported by the individual RT-qPCR results from 20 saliva samples, where two samples did not show the expected result for the N1 region but tested positive for the N2 region. Therefore, the N1 region of both samples could correspond to any nucleotide combination from SARS-CoV-2 variants without 100% identity with both frequency thresholds. In a RT-qPCR experiment, two reactions may show similar Ct values but different fluorescence signals, under different conditions[37]. Moreover, the implementation of 60 mM of TMAC, improves Illumina sequencing libraries preparation from AT-biased genomes[38] and avoids non-specific amplification in the Loop-mediated isothermal amplification, LAMP[39]. In addition to above, it has been demonstrated that the addition of 3-5% of DMSO in PCR reactions, enhances the amplification of regions with high GC% content[40,41].

In accordance with that, even though Ct values did not show statistically significant differences, which may be due to the viral load of the sample or the integrity of the viral RNA and the presence of canonical and non-canonical sub-genomes[42]; an increase in fluorescence signal was observed when DS was implemented, which indicates that the DS improves the polymerization signal despite the RNA amount present in the sample. To confirm this, sequencing of the samples is necessary to establish the nucleotide organization and potential variant presence.

These findings were further validated with multiplex RT-qPCR in pooled samples, where the fluorescent signal was proportional to the increase in positive samples compared to negatives. This result was attributed to the fact that the probes for the N1 and N2 regions had the same fluorophore [FAM] in the same RT-qPCR, leading to a cumulative increase in signal with each RT-qPCR cycle.

Considering that SARS-CoV-2 is primarily transmitted through saliva aerosols generated during coughing, sneezing, and speaking [17,43], obtaining saliva samples for detection through RT-qPCR provides a representative and cost-effective solution with a substantially increased patient acceptance compared to nasopharyngeal sampling, as demonstrated previously [17,18,20].

Conclusion

The addition of DS in RT-qPCR for individual or pooled saliva pooled samples offers a rapid, simple, and easily applicable improvement in polymerization signal, thereby contributing significantly to the SARS-CoV-2 CDC procedure by eliminating RNA stem-loop structures from the *N* gene regions employed for its detection.

Authors' contributions

LMVC: samples acquisition and analysis, results interpretation, manuscript writing and final revision. Approval of the manuscript final version. NANB: samples processing, data analysis, manuscript writing and final revision. Approval of the manuscript final version. YSCU: statistical analysis, results interpretation, manuscript writing and final revision. Approval of the manuscript final version. LAPD: secondary structures analysis, results interpretation, manuscript writing and final revision. Approval of the manuscript final version. CECC: samples processing, data analysis, results interpretation, manuscript writing and final revision. Approval of the manuscript final version. CJBH: data analysis and computing processing, manuscript writing and final revision. Approval of the manuscript final version. FMP: samples acquisition and processing, methodology design, results interpretation, manuscript writing and final revision. Approval of the manuscript final version.

Acknowledgements

The authors would like to express their gratitude, especially to the Laboratorio Central de Investigaciones de la Facultad de Salud de la Universidad Industrial de Santander, for providing access to saliva samples and laboratory facilities. In addition, we thank Michelle N. Vega-Parra for her collaboration in the final manuscript edition.

Ethical Considerations

This research was approved by the Comité de Ética en Investigación *Científica* (CEINCI) of the Universidad Industrial de Santander, as recorded in Acta No. 1 dated February 10, 2023, for saliva sample collection, and in Acta No. 5 from a virtual meeting held on April 13, 2020 for the experimental procedures. Moreover, the study was conducted in full compliance with the bioethical principles outlined in the Declaration of Helsinki (2013) and with the guidelines of the Committee on Publication Ethics (COPE).

Conflict of interest

The authors declare that they have no conflict of interest in the publication of this article.

Funding

This research was supported by the Ministerio de Ciencia Tecnología e Inovación de Colombia (Minciencias) under contract No. 369-2020, code 1102101576900, and by the Universidad Industrial de Santander through project No. 76900.

AI technological support

No artificial intelligence, language modeling or machine learning was used in the creation of this article.

Supplementary material

The supplementary material used in this work is deposited in a Zenodo repository and can be found in: https://doi.org/10.5281/zenodo.17436325

References

1. Zhu N, Zhang D, Wang W, Li X, Yang B, Song J, et al. A novel coronavirus from patients with pneumonia in China, 2019. N Engl J Med. 2020; 382(8): 727-33. doi: https://doi.org/10.1056/NEJMoa2001017

2. Adil MT, Rahman R, Whitelaw D, Jain V, Al-Taan O, Rashid F, et al. SARS-CoV-2 and the pandemic of COVID-19. Postgrad Med J. 2021; 97(1144): 110-6. doi: https://doi.org/10.1136/postgradmedj-2020-138386

3. Nakagawa S, Miyazawa T. Genome evolution of SARS-CoV-2 and its virological characteristics. Inflamm Regen. 2020; 40: 17. doi: https://doi.org/10.1186/s41232-020-00126-7

4. Corman VM, Landt O, Kaiser M, Molenkamp R, Meijer A, Chu DK, et al. Detection of 2019 novel coronavirus (2019-nCoV) by real-time RT-PCR. Euro Surveill. 2020; 25(3). doi: https://doi.org/10.2807/1560-7917.ES.2020.25.3.2000045

5. Butler KS, Carson BD, Podlevsky JD, Mayes CM, Rowland JM, Campbell DA, et al. Singleplex, multiplex and pooled sample real-time RT-PCR assays for detection of SARS-CoV-2 in an occupational medicine setting. Sci Rep. 2022; 12(1). doi: https://doi.org/10.1038/s41598-022-22106-2

6. Lu X, Wang L, Sakthivel SK, Whitaker B, Murray J, Kamili S, et al. US CDC real-time reverse transcription PCR panel for detection of severe acute respiratory syndrome coronavirus 2. Emerg Infect Dis. 2020; 26(8): 1654-65. doi: https://doi.org/10.3201/eid2608.201246

7. Kim HN, Yoon SY, Lim CS, Yoon J. Comparison of three molecular diagnostic assays for SARS-CoV-2 detection: evaluation of analytical sensitivity and clinical performance. J Clin Lab Anal. 2022; 36(2). doi: https://doi.org/10.1002/jcla.24242

8. Kuzan A, Tabakov I, Madej L, Mucha A, Fulawka L. What to do if the qPCR test for SARS-CoV-2 or other pathogen lacks endogenous internal control? A simple test on housekeeping genes. Biomedicines. 2023; 11(5): 1337. doi: https://doi.org/10.3390/biomedicines11051337

9. Benevides L, Mesquita FP, Brasil de Oliveira LL, Andréa da Silva Oliveira F, Elisabete Amaral de Moraes M, Souza PFN, et al. True or false: what are the factors that influence COVID-19 diagnosis by RT-qPCR? Expert Rev Mol Diagn. 2022; 22(2): 157-67. doi: https://doi.org/10.1080/14737159.2022.2037425

10. Bustin S, Huggett J. qPCR primer design revisited. Biomol Detect Quantif. 2017; 14: 19-28. doi: https://doi.org/10.1016/j.bdq.2017.11.001

11. Georgakopoulos-Soares I, Chan CSY, Ahituv N, Hemberg M. High-throughput techniques enable advances in the roles of DNA and RNA secondary structures in transcriptional and post-transcriptional gene regulation. Genome Biol. 2022; 23: 159. doi: https://doi.org/10.1186/s13059-022-02727-6

12. Condé L, Allatif O, Ohlmann T, de Breyne S. Translation of SARS-CoV-2 gRNA is extremely efficient and competitive despite a high degree of secondary structures and the presence of an uORF. Viruses. 2022; 14(7): 1505. doi: https://doi.org/10.3390/v14071505

13. Kelly JA, Olson AN, Neupane K, Munshi S, San Emeterio J, Pollack L, et al. Structural and functional conservation of the programmed -1 ribosomal frameshift signal of SARS-CoV-2. J Biol Chem. 2020; 295(31): 10741-8. doi: https://doi.org/10.1074/jbc.AC120.013449

14. Kovářová M, Dráber P. New specificity and yield enhancer of polymerase chain reactions. Nucleic Acids Res. 2000; 28(13): e70. doi: https://doi.org/10.1093/nar/28.13.e70

15. Cadena-Caballero CE, Vera-Cala LM, Barrios-Hernández C, Rueda-Plata D, Forero-Buitrago LJ, Torres-Jimenez CS, et al. Denaturing and dNTPs reagents improve SARS-CoV-2 detection via single and multiplex RT-qPCR. F1000Res. 2022; 11: 331. doi: https://doi.org/10.12688/f1000research.109673.2

16. Marra P, Colacurcio V, Bisogno A, de Luca P, Calvanese M, Petrosino M, et al. Evaluation of discomfort in nasopharyngeal swab specimen collection for SARS-CoV-2 diagnosis. Clin Ter. 2021; 172(5): 448-52. doi: https://doi.org/10.7417/CT.2021.2357

17. Jung EJ, Lee SK, Shin SH, Kim JS, Woo H, Cho EJ, et al. Comparison of nasal swabs, nasopharyngeal swabs, and saliva samples for the detection of SARS-CoV-2 and other respiratory virus infections. Ann Lab Med. 2023; 43(5): 434-42. doi: https://doi.org/10.3343/alm.2023.43.5.434

18. Dutta D, Naiyer S, Mansuri S, Soni N, Singh V, Bhat KH, et al. COVID-19 diagnosis: a comprehensive review of the RT-qPCR method for detection of SARS-CoV-2. Diagnostics. 2022; 12(6): 1503. doi: https://doi.org/10.3390/diagnostics12061503

19. Daniel EA, Esakialraj LBH, SA, Muthuramalingam K, Karunaianantham R, Karunakaran LP, et al. Pooled testing strategies for SARS-CoV-2 diagnosis: a comprehensive review. Diagn Microbiol Infect Dis. 2021; 101(2): 115432. doi: https://doi.org/10.1016/j.diagmicrobio.2021.115432

20. Alacam S, Bakir A. Pooling strategy for detection of SARS-CoV-2 RNA by real-time RT-PCR: comparison of pooling 5 and 10 samples. Clin Lab. 2023; 69(8): 1617-21. doi: https://doi.org/10.7754/Clin.Lab.2023.220830

21. World Medical Association Declaration of Helsinki. JAMA. 2013; 310(20): 2191-4. doi: https://doi.org/10.1001/jama.2013.281053

22. Cadena-Caballero CE, Navarro-Corredor MA, Vera-Cala LM, Barrios-Hernández C, Torres-Jiménez CS, Pardo-Diaz LA, et al. The nucleotides absent in genes of SARS-CoV-2 non-canonical subgenomic RNAs generate new programmed -1 ribosomal frameshifting. Zenodo. 2023. doi: https://doi.org/10.5281/zenodo.10398316

23. Wu F, Zhao S, Yu B, Chen YM, Wang W, Song ZG, et al. A new coronavirus associated with human respiratory disease in China. Nature. 2020; 579(7798): 265-9. doi: https://doi.org/10.1038/s41586-020-2008-3

24. Tamura K, Stecher G, Kumar S. MEGA11: Molecular evolutionary genetics analysis version 11. Mol Biol Evol. 2021; 38(7): 3022-7. doi: https://doi.org/10.1093/molbev/msab120

25. Zuker M. Mfold web server for nucleic acid folding and hybridization prediction. Nucleic Acids Res. 2003; 31(13): 3406-15. doi: https://doi.org/10.1093/nar/gkg595

26. Darty K, Denise A, Ponty Y. VARNA: interactive drawing and editing of the RNA secondary structure. Bioinformatics. 2009; 25(15): 1974-5. doi: https://doi.org/10.1093/bioinformatics/btp250

27. Biesiada M, Purzycka KJ, Szachniuk M, Blazewicz J, Adamiak RW. Automated RNA 3D structure prediction with RNAComposer. Methods Mol Biol. 2016; 1490: 199-215. doi: https://doi.org/10.1007/978-1-4939-6433-8_13

28. R Core Team. R: a language and environment for statistical computing. Vienna: R Foundation for Statistical Computing; 2021.

29. RStudio Team. RStudio: integrated development for R. Boston: RStudio; 2020.

30. Jiang W, Ji W, Zhang Y, Xie Y, Chen S, Jin Y, et al. An update on detection technologies for SARS-CoV-2 variants of concern. Viruses. 2022; 14(11): 2324. doi: https://doi.org/10.3390/v14112324

31. Aguilar R, Mardones C, Moreno AA, Cepeda-Plaza M. A guide to RNA structure analysis and RNA-targeting methods. FEBS J. 2024;. doi: https://doi.org/10.1111/febs.17368

32. Wedemeyer H, Leus M, Battersby TR, Glenn J, Gordien E, Kamili S, et al. HDV RNA assays: performance characteristics, clinical utility, and challenges. Hepatology. 2023;. https://pubmed.ncbi.nlm.nih.gov/37640384

33. Wong JLC, David S, Sanchez-Garrido J, Woo JZ, Low WW, Morecchiato F, et al. Recurrent emergence of *Klebsiella pneumoniae* carbapenem resistance mediated by an inhibitory ompK36 mRNA secondary structure. Proc Natl Acad Sci U S A. 2022; 119(38). doi: https://doi.org/10.1073/pnas.2203593119

34. Day WHE, McMorris FR. Threshold consensus methods for molecular sequences. J Theor Biol. 1992; 159(4): 481-9. doi: https://doi.org/10.1016/S0022-5193(05)80692-7

35. Lesbon J, Poleti M, de Mattos Oliveira E, Patané J, Clemente L, Viala V, et al. Nucleocapsid (*N*) gene mutations of SARS-CoV-2 can affect real-time RT-PCR diagnostic and impact false-negative results. Viruses. 2021; 13(12): 2474. doi: https://doi.org/10.3390/v13122474

36. Hamill V, Noll L, Lu N, Tsui WNT, Porter EP, Gray M, et al. Molecular detection of SARS-CoV-2 strains and differentiation of Delta variant strains. Transbound Emerg Dis. 2022; 69(5): 2879-89. doi: https://doi.org/10.1111/tbed.14443

37. Nagy A, Vitásková E, Černíková L, Křivda V, Jiřincová H, Sedlák K, et al. Evaluation of TaqMan qPCR system integrating two identically labelled hydrolysis probes in a single assay. Sci Rep. 2017; 7(1). doi: https://doi.org/10.1038/srep41392

38. Oyola SO, Otto TD, Gu Y, Maslen G, Manske M, Campino S, et al. Optimizing Illumina next-generation sequencing library preparation for extremely AT-biased genomes. BMC Genomics. 2012; 13: 1. doi: https://doi.org/10.1186/1471-2164-13-1

39. Jang M, Kim S. Inhibition of non-specific amplification in loop-mediated isothermal amplification via tetramethylammonium chloride. Biochip J. 2022; 16(3): 326-33. doi: https://doi.org/10.1007/s13206-022-00070-3

40. Yang Z, Yang J, Yue L, Shen B, Wang J, Miao Y, et al. Enhancement effects and mechanism studies of two bismuth-based materials assisted by DMSO and glycerol in GC-rich PCR. Molecules. 2023; 28(11): 4515. doi: https://doi.org/10.3390/molecules28114515

41. Varadharajan B, Parani M. DMSO and betaine significantly enhance the PCR amplification of ITS2 DNA barcodes from plants. Genome. 2020; 64(3): 165-71. doi: https://doi.org/10.1139/gen-2019-0221

42. Chen Z, Ng RWY, Lui G, Ling L, Chow C, Yeung ACM, et al. Profiling of SARS-CoV-2 subgenomic RNAs in clinical specimens. Microbiol Spectr. 2022; 10(2). doi: https://doi.org/10.1128/spectrum.00182-22

43. Stadnytskyi V, Anfinrud P, Bax A. Breathing, speaking, coughing or sneezing: what drives transmission of SARS-CoV-2? J Intern Med. 2021; 290(5): 1010-27. doi: https://doi.org/10.1111/joim.13326